ISAS - INTERNATIONAL SCHOOL
FOR ADVANCED STUDIES

Ab-initio dynamical properties of Be (0001) surface

Thesis submitted for the degree of

"Magister Philosophiæ"

CANDIDATE

Michele Lazzeri

SUPERVISOR

Stefano de Gironcoli

October 1997

SISSA - SCUOLA
NTERNAZIONALE
SUPERIORE
I STUDI AVANZATI

TRIESTE
Via Beirut 2-4

TRIESTE

SISSA ISAS
SCUOLA INTERNAZIONALE SUPERIORE DI STUDI AVANZATI
INTERNATIONAL SCHOOL FOR ADVANCED STUDIES

Ab-initio dynamical properties of Be (0001) surface

Thesis submitted for the degree of

"Magister Philosophiæ"

CANDIDATE

Michele Lazzeri

SUPERVISOR

Stefano de Gironcoli

October 1997

Index

Introduction

The study of dynamical properties of matter is motivated by the quest for a detailed understanding of the forces between atoms, thus in the last forty years bulk phonons have been studied with this aim both experimentally and theoretically. An important check of our understanding is the comparison between bulk and surface properties of a material. The lower particle coordination and the different symmetry at the surface can lead to a different behaviour with respect to the bulk which can be a stringent test for the transferability of models used to interpret atom interactions [1].

In recent years advances in experimental technique such as electron energy loss spectroscopy (EELS) and low energy He atom scattering have made available a great deal of data for clean crystal surfaces of many materials, which interpretation is in many cases still challanging [1]. This is indeed the case of Beryllium surfaces which have recently attracted much experimental and theoretical attention [2, 3, 4, 5, 6, 7, 8, 9, 10].

Be is the second row and second column element in the periodic table; it is a strongly bound metal, stable in *hcp* crystalline structure. Its four electrons, in the ground state for isolated atom, have orbitals 1S and 2S, and to have a bond outermost orbitals have to hybridize to p-states. Bonding has a partially covalent character more marked than other

elements of the same column. Be (0001) surface presents an anomalous character: its first layer relaxes outward by several percents (this behaviour is not a common one for metals) and its density of electronic states, that has a peak near the Fermi energy, seems to be more metallic than the bulk itself. Both this features contribute to strange dynamical properties that have recently been measured, using EELS by the group of Plummer [5, 6].

Early attempts to interpret this data using accurate bulk-truncated models have failed [6] giving even a qualitative disagreement: as we will show they predict wrong sign for the dispersion of the lowest energy mode(Rayleigh Wave) in some high symmetry direction. Evidently the marked difference between properties of this surface with respect to the bulk crystal make it diffcult to use phoenomenological models, this fact has driven us to face the problem using first principles calculation.

We have used density functional theory (DFT) [11] with the local density approximation (LDA) for the exchange-correlation energy and density functional perturbation theory (DFPT). DFPT provides a general theoretical tool for obtaining the harmonic force constants of complex systems fully *ab initio* without the use of any adjustable parameter. This method gives access to the phonon frequencies and the corresponding atomic displacement patterns at any point in the Brillouin zone (BZ), allowing us to calculate full phonon dispersions. This technique has been successfully applied to predict vibrational and related properties of elemental and binary semiconductors [12] or insulators [13], semiconductor alloys [14] and eterostructures [15], and more recently to the calculation of phonon dispersion in bulk metals [16] and surfaces [17].

The last part of the work will be dedicated to the study of thermal properties of this

surface. As already said, one of the most unusual properties of Be 0001 surface is its outward interlayer relaxation, that has been confirmed by experiments and calculations [2, 9, 8, 3]. However there is a quantitative disagreement on the amount of the displacement of the first layer of this surface. Traying to clarify discrepancies arosen between experimets and theoretical calculations Pohl *et al.* [3] has revealed a strong dependence of this displacement on temperature.

We will show that DFPT with the local density approximation is a fully adequate instrument in reproducing bulk and, that's more important, surface dynamical properties. So we will deal with the problem of thermal expansion within the quasi harmonic approximation scheme.

In Chapter 1 we will focus our attention on the main characteristic of Beryllium and will explain the problems encountered in interpreting recent experimantal data.

In Chapter 2 we will give an account of the theoretical tools used for our *Ab initio* calculation of crystal dynamical properties.

In Chapter 3 we will show and discuss our results.

1 Unusual properties of Be(0001) surface

Berylium surfaces have recently attracted much experimental and theoretical attention [2, 3, 4, 5, 6, 7, 8, 9, 10], because they display markedly different properties with respect to the bulk ones. In this chapter we will show some problems recently arosen in studying Be(0001) surface.

Beryllium forms in the hexagonal-close-packed (hcp) structure with strongly contracted c/a ratio and a low density of states at the Fermi energy. Both features are related to partially covalent bonding, arising from hybridization of the atomic $2s$- and $2p$-states, that is strongly dependent on the local atomic coordination. In the close-packed (0001) surface the top layer relaxes outward by several percents [2, 3] -this is not a common behaviour for metal surfaces-, and the presence of electronic surface states[4] makes the density of states more free-electron-like and very different from the bulk one (Fig. 1.1). Surface vibrations are expected to reflect these changes.

1.1 Dynamical properties

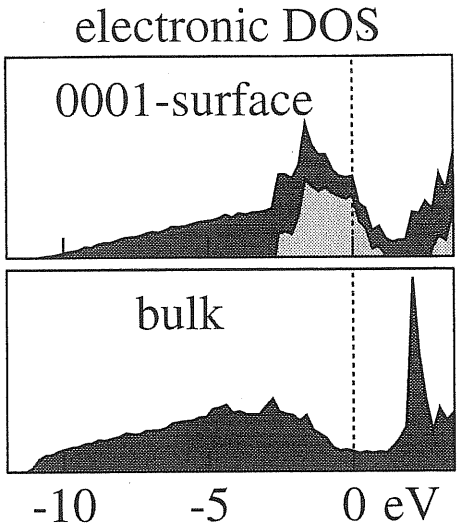

Figure 1.1: Comparison between calculated electronic density of states (DOS) of Be bulk and (0001) surface. Bulk DOS has a minimum near the Fermi energy that make it resamble the DOS of a semiconductor. Surface DOS has a more metallic character than the bulk one.

Surface-phonon dispersions at the Be (0001) surface have been recently obtained by Electron Energy Loss Spectroscopy (EELS) [5, 6], which are significantly different from calculated ones, based on truncated bulk models[6] (Fig. 1.2). With *bulk truncated model* it is meant a model in which force constants are calculated for the bulk and the force-constants so obtained are used to modellize the interaction between atoms at the surface. There is even qualitative disagreement between theory and experiment, in particular the sign of the Rayleigh wave (RW) dispersion from $\overline{K}$ to $\overline{M}$ point in the surface BZ is incorrectly given by the model calculation. This feature has been interpreted [6] as due to a reduction at the surface—related to its more free-electron-like character—of the non-central interatomic forces needed to describe the bulk vibrational properties [18].

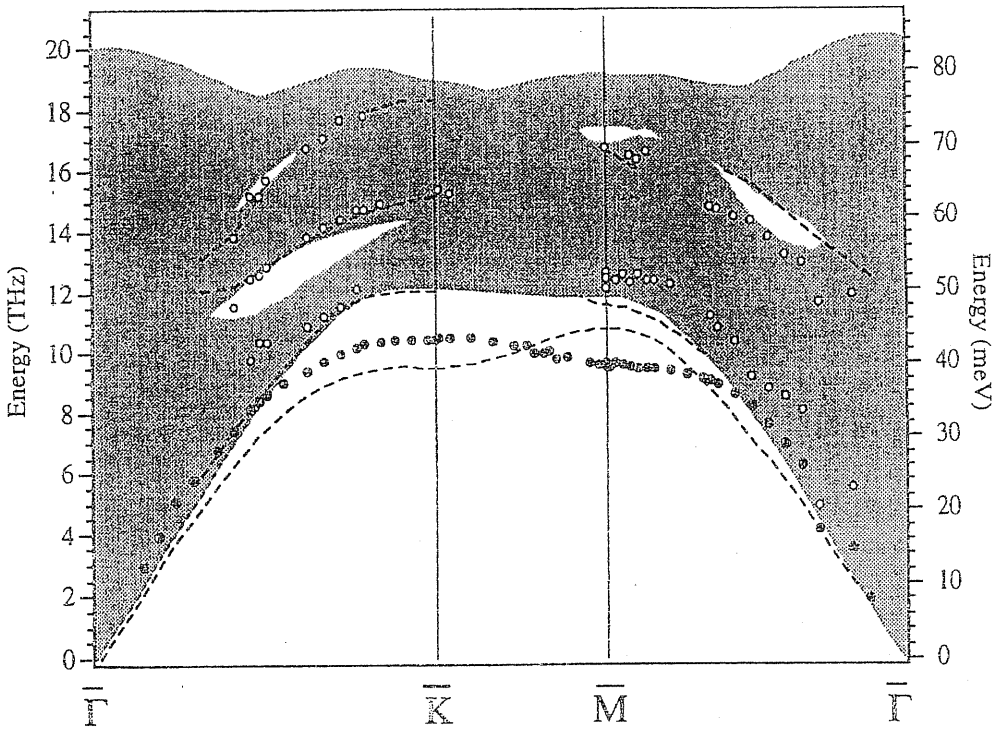

Figure 1.2: Be (0001) surface phonon from EELS [5, 6]. The filled (open) circles indicate intense (weak) features in the measured dispersion. Solid lines indicate the calculated dispersion of surface modes for a bulk-terminated slab. The shaded area corresponds to the projection of bulk phonon modes onto (0001) surface (Fig. from [6]).

1.2 Thermal expansion

It is well established that the first interlayer separation on most metal surfaces is contracted at room temperature, with only a few exceptions reported so far. Beryllium (0001) surface is one of these interesting exceptions [2]. Until very recently there was a substantial disagreement between experimental and first-principles theoretical [9, 8, 10] results on the amount of topmost interlayer expansion in this system, theoretical calculations giving roughly half of the observed value. In a recent letter, Pohl *et al.*[3] reconcile experiment and theory on this point showing that low temperature (110 K) low-energy electron diffraction (LEED) determinations of the first interlayer separation are in agreement with first-principles (zero temperature, static) calculations and that reported discrepancies at room temperature originate from a large thermal expansion of the top layer, reaching 6.7% at 700 K. These findings are very interesting and puzzling, since surface phonons show no sign of enhanced anharmonicity [6, 3]. The calculation of the surface thermal expansion [3], within a simplified quasiharmonic approach recently introduced in Ref. [19, 20], results in very good agreement with experimental findings. However, the validity of such an approach has been criticized by some authors [21], in particular because of the very poor sampling of vibrational modes adopted in the free energy calculation.

2 Theoretical tools

The study of the structural, electronic and vibrational properties of the system investigated in this thesis, has been performed within *ab initio* methods based on density functional theory. At zero temperature, the properties we are interested in can be determined starting from the knowledge of the quantum-mechanical electronic ground-state. It is obviously impossible to solve exactly the many-body Schrödinger equations of electrons and nuclei in a crystal, but an approximation universally used in solid state physics, known as the Born-Oppenheimer approximation, allows to decouple the "fast" electronic variables from the "slow" ionic ones, by virtue of the great difference of masses. The system is thus divided in two subsytems: the electrons move in the potential of the fixed nuclei, following adiabatically their slow motion and remaining always close to the quantum-mechanical ground state, while the ions are treated as if they were classical particles in the effective potential determined by the electronic ground state.

DFT provides a theoretical framework to describe the electronic ground-state of a solid, without having to solve the Schrödinger equation for the quantum many-electron system, which would be an impossible task due to the very large number of degrees of freedom involved in the calculation.

2.1 Density functional theory

This theory was developed 30 years ago on the basis of the Hohenberg-Kohn theorem [22], which proofs the uniqueness of the external potential acting on the subsystem of the electrons as a functional of the electronic density $n(\mathbf{r})$. The energy of the electrons can be written as

$$E[n(\mathbf{r})] = F[n(\mathbf{r})] + \int V(\mathbf{r})n(\mathbf{r})d\mathbf{r}, \tag{2.1}$$

where $F[n]$ is a universal functional of the electronic density (independent on the external potential), and $V(\mathbf{r})$ is the "external" potential (with respect to the electrons) generated by the ionic cores.

In principle this problem should be solved via the constrained minimization of this functional, in general unknown, with respect to the electron density, that must always be normalized to the number N of electrons:

$$\int n(\mathbf{r})d\mathbf{r} = N. \tag{2.2}$$

In order to apply this theory to actual calculations, Kohn and Sham proposed to separate the functional $F[n]$ into three distinct contributes:

$$F[n(\mathbf{r})] = T_0[n(\mathbf{r})] + \frac{1}{2}\int \frac{n(\mathbf{r})n(\mathbf{r}')}{|\mathbf{r}-\mathbf{r}'|}d\mathbf{r}d\mathbf{r}' + E_{xc}[n(\mathbf{r})]. \tag{2.3}$$

$T_0[n(\mathbf{r})]$ is the kinetic energy of a system of noninteracting electrons of density $n(\mathbf{r})$, the second is the classical Hartree term describing the Coulomb potential of the electrons, while $E_{xc}[n(\mathbf{r})]$, defined by this formula, is known as the exchange and correlation energy and contains all the information about the many-body interactions among electrons that we do not know.

This way, the problem of constrained minimization becomes the problem of solving a set of self-consistent single particle equations:

$$\underbrace{\left[-\frac{\nabla^2}{2} + V_{SCF}(\mathbf{r})\right]}_{H_{KS}} \psi_i(\mathbf{r}) = \epsilon_i \psi_i(\mathbf{r}) \tag{2.4}$$

$$V_{SCF}(\mathbf{r}) = V(\mathbf{r}) + \int \frac{n(\mathbf{r}')}{|\mathbf{r} - \mathbf{r}'|} d\mathbf{r}' + v_{xc}[n(\mathbf{r})] \tag{2.5}$$

$$n(\mathbf{r}) = \sum_i |\psi_i(\mathbf{r})|^2 \, \theta(\epsilon_i - \epsilon_F). \tag{2.6}$$

These are the well known Kohn-Sham (KS) equations [23], where the Fermi energy ϵ_F is defined by the constraint on the number of electrons, $v_{xc}(\mathbf{r}) = \delta E_{xc}[n]/\delta n(\mathbf{r})$ is the exchange-correlation potential and the single particle orbitals satisfy the orthonormality constraint $\int \psi_i^*(\mathbf{r})\psi_j(\mathbf{r})d\mathbf{r} = \delta_{ij}$.

2.1.1 The local-density approximation

The Kohn-Sham equations are exact and still contain a completely unknown term in the exchange-correlation potential . In order to face this problem it is necessary, at this point, to introduce some approximations. A very natural approximation to DFT is the well-known local density approximation (LDA), in which the exchange-correlation energy is taken as a local *function* rather than a functional of the density:

$$E_{xc}[n(\mathbf{r})] = \int n(\mathbf{r}) \epsilon_{xc}(n(\mathbf{r})) \, d\mathbf{r}, \tag{2.7}$$

and the potential is given by:

$$v_{xc}(\mathbf{r}) = \frac{d}{dn}(n(\mathbf{r})\epsilon_{xc}(n(\mathbf{r}))) = \mu_{xc}(n(\mathbf{r})). \tag{2.8}$$

In this approximation, the total energy of the crystal in its electronic ground state is:

$$\begin{aligned} E^{tot} &= -\sum_i \theta(\epsilon_i - \epsilon_F) \int \psi_i^*(\mathbf{r}) \nabla^2 \psi_i(\mathbf{r}) d\mathbf{r} + \int V_{ion}(\mathbf{r}) n(\mathbf{r}) d\mathbf{r} \\ &+ \frac{1}{2} \int \frac{n(\mathbf{r}) n(\mathbf{r}')}{|\mathbf{r} - \mathbf{r}'|} d\mathbf{r} d\mathbf{r}' + \int n(\mathbf{r}) \epsilon_{xc}(n(\mathbf{r})) d\mathbf{r} \\ &+ \sum_{\mathbf{R},s,s'}{}' \frac{Z_s Z_{s'}}{|\mathbf{R} + \tau_s - \tau_{s'}|} . \end{aligned} \tag{2.9}$$

LDA works surprisingly well for a large variety of systems, even more than any possible expectations, but it is known to be worse when describing weak atomic bondings. In the last decade, a lot of improvements to LDA were proposed [24, 25, 26, 27], but none of them seems to be a real "breakthrough" in this direction.

They are mostly based on the inclusion, in the dependence of the exchange and correlation functional, not only of the electronic density, but also of its gradient, and even of the Laplacian. For this reason they are commonly known as gradient-correction approximations (GCA). These kinds of new functionals are not fully satisfactory from a theoretical point of view, but certainly are able to describe better those situations in which LDA breaks down.

2.1.2 The plane-wave pseudopotential method

The actual solution of the KS equations can be obtained expanding the KS wavefunctions on a basis set. The most widely used choice of this basis is that of plane waves (PW), which have the great advantage of being translationally invariant:

$$\psi_i(\mathbf{r}) = \psi_{n,\mathbf{k}}(\mathbf{r}) = \sum_{\mathbf{G}} e^{i(\mathbf{k}+\mathbf{G})\mathbf{r}} c_n(\mathbf{k} + \mathbf{G}) \tag{2.10}$$

where $\mathbf{k}$ belongs to the first Brillouin Zone (BZ) of the crystal, $\mathbf{G}$ is a reciprocal lattice vector and n is the band index. The PW basis set is infinite and it is usually truncated by

choosing a kinetic energy cutoff through the condition:

$$|\mathbf{k}+\mathbf{G}|^2 \leq E_{cut}. \tag{2.11}$$

To treat explicitly all the electrons it would be necessary to choose a very large number of PW in order to describe accurately their rapid oscillations near the nucleus. This would require a very heavy computational effort for the calculation. It is possible to avoid this problem freezing the core electrons in the atomic configuration around the ions, and considering only the valence electrons.

To do this, one introduces the *pseudopotentials*, able to describe the interactions between these electrons and the *pseudoions* (ions+ core electrons). The valence electrons wavefunctions are considerably smoother near the nucleus, but are identical to the "true" wavefunctions outside the core region. This method is now well-established in computational physics, and the results are very accurate.

The widely-used norm-conserving pseudopotentials [28] consist of a local contribution for the radial function and a non-local one for the angular part:

$$v_s(\mathbf{r},\mathbf{r}') = v_s^{loc}(r)\delta(\mathbf{r}-\mathbf{r}') + \sum_{l=0}^{l_{max}} v_{s,l}(r)\delta(r-r')P_l(\hat{\mathbf{r}},\hat{\mathbf{r}}'), \tag{2.12}$$

where P_l is the projector on the angular momentum l.

This form of *semilocal* pseudopotential still is not the most convenient one from a computational point of view, and for this reason Kleinman and Bylander (KB) introduced [29] a fully non-local pseudopotential in which also the radial part of the potential is non-local:

$$v_s^{(NL)}(\mathbf{r},\mathbf{r}') = v_s^{loc}(r)\delta(\mathbf{r}-\mathbf{r}') + \sum_{l=0}^{l_{max}} v_{s,l}^{(NL)}(\mathbf{r},\mathbf{r}'), \tag{2.13}$$

where

$$v_{s,l}^{(NL)}(\mathbf{r},\mathbf{r}') = \sum_{m=-l}^{l} \frac{v_{s,l}(r)R_{s,l}(r)Y_l^m(\theta,\phi)Y_l^{*m}(\theta',\phi')R_{s,l}(r')v_{s,l}(r')}{\langle R_{s,l}|v_{s,l}|R_{s,l}\rangle}. \tag{2.14}$$

This form of the potential allows a very convenient simplification of its matrix elements in reciprocal space, where the KS equations are iteratively solved.

2.1.3 Non linear core correction

The idea underlying NLCC is to use the *total* charge instead of the *valence* charge to compute the exchange-correlation energy [30]:

$$E_{xc} = \int_V d\mathbf{r}\epsilon_{xc}(n_v + n_c)(n_v + n_c), \tag{2.15}$$

where n_c is the charge density of the core electrons, computed as a superposition of the atomic core charges of the atoms which requires NLCC and n_v is the valence charge. The core charge is computed only once, together with the psuedopotential and then it is added to the valence charge to compute the exchange-correlation energy.

2.2 Lattice dynamics

Phonons are normal modes of the harmonic lattice vibrations. Within the *adiabatic* approximation, the lattice dynamics can be studied as if the ions were classical charges moving in an effective potential determined by the ground-state electronic energy. Therefore the total energy, as a function of the coordinates, plays the role of a potential surface for the atomic motion. For small displacements of atoms around their equilibrium positions, $\mathbf{u}_s(\mathbf{R})$, the total energy of the crystal can be expanded in a Taylor series, which up to second order

would read:

$$E^{tot}[\mathbf{u}] = E_o^{tot} + \frac{1}{2}\sum_{\mathbf{R}s,\mathbf{R}'s'} \frac{\partial^2 E^{tot}}{\partial \mathbf{u}_s(\mathbf{R})\partial \mathbf{u}_{s'}(\mathbf{R}')}\mathbf{u}_s(\mathbf{R})\mathbf{u}_{s'}(\mathbf{R}') + \mathcal{O}(\mathbf{u}^3). \tag{2.16}$$

The linear terms vanish because of equilibrium. E_0^{tot} is the total energy of the crystal at equilibrium, and $\mathbf{u}_s(\mathbf{R})$ is the displacement of the s-th atom in the unit cell located at $\mathbf{R}$. Within this picture, the harmonic oscillations around equilibrium positions are governed by the equations of motions:

$$M_s\ddot{u}_{\alpha s}(\mathbf{R}) = -\frac{\partial E^{tot}}{\partial u_{\alpha s}(\mathbf{R})} = -\sum_{\mathbf{R}',s',\beta} C_{\alpha s,\beta s'}(\mathbf{R}-\mathbf{R}')u_{\beta s'}(\mathbf{R}'), \tag{2.17}$$

where M_s is the mass of the s-th atom, and $\alpha,\beta = x,y,z$ are the polarizations. The interatomic force constants are given by:

$$C_{\alpha s,\beta s'}(\mathbf{R}-\mathbf{R}') = \frac{\partial^2 E^{tot}}{\partial \mathbf{u}_{\alpha s}(\mathbf{R})\partial \mathbf{u}_{\beta s'}(\mathbf{R}')}, \tag{2.18}$$

where the second derivatives are calculated at equilibrium. $C_{\alpha s,\beta s'}(\mathbf{R}-\mathbf{R}')$ represents the negative of the linear force on atom s in the cell at $\mathbf{R}$ along the α direction due to a unit displacement of atom s' in the cell at $\mathbf{R}'$ along the β direction. The force constants are connected to each other by relations due to symmetry properties of the crystal. In particular they only depend on the difference $\mathbf{R}-\mathbf{R}'$ because of the translational invariance of the crystal. Thanks to translational invariance,the solutions of the infinite set of coupled equations 2.17 are waves:

$$\mathbf{u}_s(\mathbf{R}) = \frac{1}{\sqrt{M_s}}\mathbf{u}_s(\mathbf{q})e^{i\mathbf{q}\mathbf{R}-i\omega t}, \tag{2.19}$$

where the wave vector $\mathbf{q}$ belongs to the Brillouin zone. Once the dynamical matrix is known, the problem of solving the lattice dynamics is reduced to a $3N_{at}\times 3N_{at}$ (number of atoms)

eigenvalue problem :

$$\omega^2 \mathbf{u}_s(\mathbf{q}) = \sum_{s'} \mathbf{D}_{ss'}(\mathbf{q}) \mathbf{u}_{s'}(\mathbf{q}) \tag{2.20}$$

The dynamical matrix $\mathbf{D}_{ss'}(\mathbf{q})$ is related to the Fourier transform of the matrix of force constants:

$$D_{\alpha s,\beta s'}(\mathbf{q}) = \frac{1}{\sqrt{M_s M_s'}} \sum_{\mathbf{R}} C_{\alpha s,\beta s'}(\mathbf{R}) e^{-i\mathbf{q}\mathbf{R}}. \tag{2.21}$$

It is a hermitian matrix, and has the well known properties [31]:

$$D_{\alpha s,\beta s'}(\mathbf{q}) = D^*_{\beta s',\alpha s}(\mathbf{q}), D_{\alpha s,\beta s'}(-\mathbf{q}) = D^*_{\alpha s,\beta s'}(\mathbf{q}) \tag{2.22}$$

For each $\mathbf{q}$ point in the BZ, the $3N_{at}$ eigenvalues of the dynamical matrix: $\omega^2_\nu(\mathbf{q})$; $\nu = 1, 2, 3, \cdots, 3N_{at}$,are positive for stable systems. Their square root gives the frequency of the $\nu - th$ vibrational normal-mode, i.e. the dispersion relations $\omega = \omega_\nu(\mathbf{q})$. The corresponding $3N_{at}$ eigenvectors $\mathbf{u}^\nu_s(\mathbf{q})$ are related to the normal-mode atomic displacements through the Eq.2.19. Every harmonic vibration of the lattice is a linear superposition of the $3N_{at}$ normal-modes.

2.2.1 *Ab initio* interatomic force constants

A complete description of the harmonic vibrations of a crystal is provided by the knowledge of the interatomic force constants. Within the adiabatic approximation, the lattice distortioin associated with a phonon can be seen as a static perturbation acting on the electrons. Furthermore, it is well known that the linear variation of the electron density upon application of an external, static, perturbation determines the energy variation up to second order in the perturbation (up to third order, indeed, as stated by the "$(2n+1)theorem$" [32]). When the external perturbation is due to ionic displacements, this allows one to calculate the

interatomic force constants which are directly obtained from the electronic linear-response to ionic displacements. In fact, the *bare* ionic (pseudo-)potential acting on the electrons is a continuous function of the atomic displacements $\mathbf{u} \equiv \{\mathbf{u}_s(\mathbf{R})\}$. The electronic contribution to the force associated with the displacement along α of the $s-th$ ion in the cell at $\mathbf{R}$ ($u_{\alpha s}(\mathbf{R})$) is given by the Hellmann-Feynman theorem [33]:

$$\frac{\partial E^{el}_{[\mathbf{u}]}}{\partial u_{\alpha s}(\mathbf{R})} = \int n_{[\mathbf{u}]}(\mathbf{r}) \frac{\partial V^{ion}_{[\mathbf{u}]}(\mathbf{r})}{\partial u_{\alpha s}(\mathbf{R})} d\mathbf{r}, \tag{2.23}$$

where $E^{el}_{[\mathbf{u}]}$ is the electronic ground-state energy relative to given values of the atomic displacements $\mathbf{u}$, and $u_{[\mathbf{u}]}$ is the corresponding electron-density distribution. The electronic contribution to the harmonic force constants is then obtained by differentiating Eq. 2.23 with respect to $\mathbf{u}_{s'}(\mathbf{R}')$:

$$\frac{\partial^2 E^{el}_{[\mathbf{u}]}}{\partial u_{\beta s'}(\mathbf{R}') \partial u_{\alpha s}(\mathbf{R})} = \int \left(\frac{\partial n_{[\mathbf{u}]}(\mathbf{r})}{\partial u_{\beta s'}(\mathbf{R}')} \frac{\partial V^{ion}_{[\mathbf{u}]}(\mathbf{r})}{\partial u_{\alpha s}(\mathbf{R})} + n_0(\mathbf{r}) \frac{\partial^2 V^{ion}_{[\mathbf{u}]}(\mathbf{r})}{\partial u_{\beta s'}(\mathbf{R}') \partial u_{\alpha s}(\mathbf{R})} \right) d\mathbf{r}, \tag{2.24}$$

where all the derivatives are calculated at the equilibrium positions, i.e. at $\mathbf{u} = 0$, $n_0(\mathbf{r})$ is the ground-state alectronic density of the unperturbed system, $V^{ion}_{[\mathbf{u}]}(\mathbf{r})$ is the bare ionic (pseudo) potential acting on the electrons:

$$V^{ion}_{[\mathbf{u}]}(\mathbf{r}) = \sum_{\mathbf{R}s} v_s(\mathbf{r} - \mathbf{R} - \tau_s - \mathbf{u}_s(\mathbf{R})), \tag{2.25}$$

and $\frac{\partial n_{[\mathbf{u}]}(\mathbf{r})}{\partial u_{\alpha s}(\mathbf{R})}$ is the linear-response of the electron density to the displacement of the $s-th$ ion in the unit cell at $\mathbf{R}$. The interatomic force constants can be written as a sum of two contributions:

$$C_{\alpha s, \beta s'}(\mathbf{R} - \mathbf{R}') = C^{el}_{\alpha s, \beta s'}(\mathbf{R} - \mathbf{R}') + C^{ion}_{\alpha s, \beta s'}(\mathbf{R} - \mathbf{R}'), \tag{2.26}$$

where the electronic contribution $\mathbf{C}^{el}_{s,s'}$ is given by Eq. 2.24, and the ionic one $\mathbf{C}^{ion}_{s,s'}$ is the second derivative of the Coulomb interaction between the ionic cores (which is essentially

the second derivative of an Ewald sum). The matrix of the interatomic force constants is conveniently calculated in reciprocal space:

$$C_{\alpha s,\beta s'}(\mathbf{R}) = \frac{1}{N}\sum_{\mathbf{q}} \tilde{C}_{\alpha s,\beta s'}(\mathbf{q}) e^{i\mathbf{q}\mathbf{R}}. \tag{2.27}$$

where N is the number of unit cells in the crystal. The electronic contribution is then written in reciprocal space as follows:

$$\tilde{C}_{\alpha s,\beta s'}(\mathbf{q}) = \int \left[\frac{\partial n(\mathbf{r})}{\partial u_{\alpha s}(\mathbf{q})}\right]^* \frac{\partial V^{ion}(\mathbf{r})}{\partial u_{\beta s'}(\mathbf{q})} d\mathbf{r} + \delta_{ss'} \int n_0(\mathbf{r}) \frac{\partial^2 V^{ion}(\mathbf{r})}{\partial u_{\alpha s}(\mathbf{q}=0)\partial u_{\beta s'}(\mathbf{q}=0)} d\mathbf{r}, \tag{2.28}$$

where $\frac{\partial V^{ion}(\mathbf{r})}{\partial u_{\alpha s}(\mathbf{q})}$ is the linear variation of the external ionic potential due to a periodic lattice distortion of wave vector $\mathbf{q}$:

$$u_{\alpha s}(\mathbf{R}) = u_{\alpha s}(\mathbf{q}) e^{i\mathbf{q}\mathbf{R}}, \tag{2.29}$$

and $\frac{\partial n(\mathbf{r})}{\partial u_{\alpha s}(\mathbf{q})}$ is the corresponding variation of the electron density. Equation 2.28 shows that the harmonic force constants of the crystal can be calculated by first-principles, once the electronic ground-state density of the unperturbed system $n_0(\mathbf{r})$, and its linear response to a lattice distortion of the form 2.29 are known.

When the unperturbed problem is solved in the framework of DFT, the electronic linear response is calculated within Density Functional Perturbation Theory [11] by solving the selfconsistent set of equations:

$$[H_{KS} + \tilde{O}_v - \epsilon_i]\Delta\psi_i(\mathbf{r}) = -\tilde{P}_c \Delta V_{SCF}(\mathbf{r})\psi_i(\mathbf{r}), \tag{2.30}$$

$$\Delta V_{SCF}(\mathbf{r})\psi_i(\mathbf{r}) = \Delta V_{ion}(\mathbf{r})\psi_i(\mathbf{r}) + 2\int \frac{\Delta n(\mathbf{r}')}{|\mathbf{r}-\mathbf{r}'|} d\mathbf{r}' + \left.\frac{dv_{xc}}{dn}\right|_{n=n_0(\mathbf{r})} \Delta n(\mathbf{r}), \tag{2.31}$$

$$\Delta n(\mathbf{r}) = 4\sum_i \psi_i^*(\mathbf{r})\Delta\psi_i(\mathbf{r}), \tag{2.32}$$

where i runs over the occupied states. In the Eqs. 2.30-2.32, in order to simplify the notation, Δf indicates the derivative with respect to the relevant ionic displacements: $\Delta f \equiv \frac{\partial f}{\partial \mathbf{u}}$. $\Delta V_{SCF}(\mathbf{r})$ is the variation of the self-consistent KS potential due to the variation of the bare ionic potential produced by the lattice distortion, and it is self-consistently related to the linear variation of the electronic density, $\Delta n(\mathbf{r})$, through the variation of the Hartree and exchange-correlation potentials (Eq. 2.31). The operators $\tilde{P}_c$ and $\tilde{O}_v$ are introduced in order to obtain a numerically stable solution: they orthogonalize the solution with respect to the occupied states and make the system 2.30 non-singular. These two operators are defined in a different way for metallic and non-metallic systems. For non-metallic solids, where empty and occupied states are separated by a finite energy gap, the projection of the perturbed orbitals over the unoccupied states many-fold is well defined, and it is the solution of Eq. 2.30, where $\tilde{P}_c$ and $\tilde{O}_v$ are defined respectively as:

$$\tilde{P}_c = 1 - \sum_v |\psi_v\rangle\langle\psi_v|, \tag{2.33}$$

$$\tilde{O}_v = \alpha \sum_v |\psi_v\rangle\langle\psi_v|, \tag{2.34}$$

where α is a constant larger than the valence energy band width, in such a way to make the linear system 2.30 non-singular. In this way only the valence states are involved in the computation of the linear variation of the charge density, without explicit introduction of the conduction states. In the case of metals, the smearing technique [34, 35] is used to deal with BZ integration in the presence of a Fermi surface, so that partially-filled states are introduced. As a consequence, empty and filled states are no more separated in energy, and the projection of $\Delta\psi_i(\mathbf{r})$ over the (partially-) unoccupied states is no longer well defined. In this case the problem is solved by introducing in Eq. 2.30 the "smeared operators" $\tilde{P}_c$

and $\tilde{O}_v$ defined as [16]:

$$\tilde{O}_v = \sum_i \alpha_i |\psi_i\rangle\langle\psi_i| \tag{2.35}$$

$$\tilde{P}_c^{(i)} = \tilde{\theta}_{Fi} - \sum_j \beta_{ij} |\psi_j\rangle\langle\psi_j| \tag{2.36}$$

$$\beta_{ij} = \tilde{\theta}_{Fi}\tilde{\theta}_{ij} + \tilde{\theta}_{Fj}\tilde{\theta}_{ji} + \alpha_j \frac{\tilde{\theta}_{Fi} - \tilde{\theta}_{Fj}}{\epsilon_i - \epsilon_j}\tilde{\theta}_{ji} \tag{2.37}$$

where $\tilde{\theta}_{Fi}$ is a smooth approximation of the step function $\theta(\epsilon_F - \epsilon_i)$, α_i being chosen in such a way that the system 2.30 is non-singular, and it is assumed to vanish when ψ_i is unoccupied, so that β_{ij} vanishes when both i and j refer to unoccupied states. Therefore only the partially filled states enter the definition of these "smeared operators", and no explicit introduction of the onoccupied states is needed in the computation of $\Delta n(\mathbf{r})$, as for the non-metallic case. A detailed description for practical implementation of force constants calculation within DFPT can be found in reference [12] for insulating systems, and in reference [16] for metals.

3 First principles calculation

In this chapter we present our first-principles calculations of the structural and dynamical properties of Be (0001) surface, as obtained by state-of-the-art density-functional perturbation theory (DFPT) [11, 36], and will compare our results with experiments. The obtained vibrational frequencies will be used to estimate Be thermal expansion within the quasi harmonic approximation for bulk and (0001) surface.

3.1 Structure and dynamical properties

3.1.1 Be bulk

As a preliminary step, we have computed the structural and lattice-dynamical properties of the bulk metal. Our calculations have been performed within the local-density approximation (LDA) [23, 37] using pseudopotentials and plane-wave (PW) basis sets. Be atoms were described by a separable pseudopotential [29] that includes non-linear core correction [30] and has been generated so as to optimally reproduce several atomic configurations [38, 39], to enhance transferability. Our basis set included PW's up to a kinetic energy cutoff of 22 Ry and BZ integrations were performed with the *smearing* technique of Ref. [35] using

the Hermite-Gauss smearing function of order one, a smearing width σ=50 mRy, and a 120-points grid in the irreducible wedge of the bulk BZ [40]. With these parameters all calculated properties were well converged. The resulting hcp lattice-constants, a and c, bulk modulus, B, and Poisson ratio, ν_P, are in good agreement with experimental results (in parenthesis): a = 4.25 (4.33) a.u., c/a = 1.572 (1.568), B=1.25 (1.1) Mbar, and ν_P=0.04 (0.02 - 0.05). Note the contracted value of c/a and the small value of the Poisson ratio, indicating rather strong and anisotropic bonding along the c axis.

In Fig. 3.1 we display the calculated phonon dispersions of bulk Be and compare them with neutron-diffraction data from Ref. [41]. The overall agreement is very good (about 1% throughout the BZ) and typical of *ab-initio* DFPT [11]. The agreement with experimental data is even better than that obtainable by *empirical* Born-von Karman scheme—as, for instance, in Ref. [6]—after extensive fitting of the experimental dispersion relations. Note that our calculations have *no* adjustable parameter and the only uncontrolled approximations are the adiabatic one and LDA to deal with electronic correlations.

3.1.2 Be (0001) surface

To describe the surface we adopted a repeated slab geometry with 12-layer Be slabs separated by a ≈25 a.u. thick vacuum region (equivalent to 8 atomic layers) to decouple the surfaces. In the BZ integrations we used a 30-point grid, obtained projecting the bulk grid on the surface BZ. Atomic positions in the slab were fully relaxed starting from the truncated bulk, keeping the in-plane lattice parameter fixed at the bulk value. Symmetry fixes atomic in-plane positions and relaxation involves only modification of the inter-layer spacing. The three outmost layers relax significantly from the bulk value, in agreement with

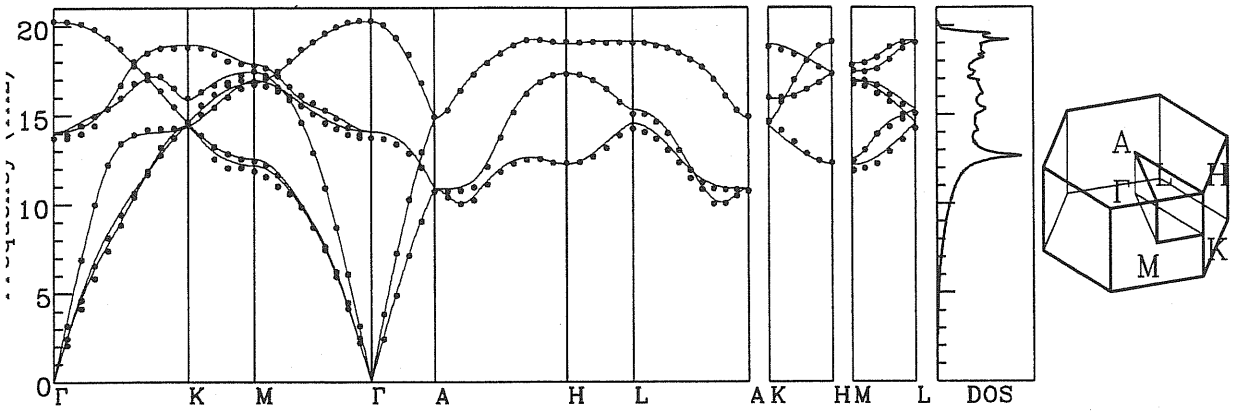

Figure 3.1: Calculated phonon dispersions for bulk Be (lines) and neutron scattering data from Ref. [41] (full dots). The calculated density of states and the hcp BZ are also shown.

experimental evidence [2, 3, 7]. The calculated values for the interlayer spacing variation are reported in Table 3.1, along with experimental data [2] and previous theoretical results. Our theoretical calculation agrees well with previous ones, but all theoretical results disagree with the LEED structural determination [2]. The use of different exchange and correlation functionals does not improve the comparison [10].

Recently the importance, in order to get close to LEED results, of including in first-principles calculations the effect of zero-point vibrations has been suggested for transiton metal surfaces [20]. In the present case, however, calculation shows (next section) that zero-point vibrations do not modify significantly the top layer relaxation. Very recently a new, low temperature (110 K), LEED determination of the structural properties of Be (0001) surface has been made [3]. The agreement between theoretical results and this new experimental determination is very good, the value for the topmost layer expansion being

Table 3.1: Relaxation of the three outer layers of Be (0001) as obtained by LEED and several electronic structure calculations. The experimental temperature is shown, while for the calculations the exchange and correlation used and the number of layers in the slab are indicated.

		$\Delta d_{12}(\%)$	$\Delta d_{23}(\%)$	$\Delta d_{34}(\%)$
Exp:	LEED (300 K)[2]	+5.8	-0.2	+0.2
Th:	LDA-12 layers, this work	+3.2	+1.0	+0.4
	LDA-11/13 layers [8]	+2.7	+1.2	+0.6
	LDA-9 layers [9]	+3.9	+2.2	
	GGA-9 layers [10]	+2.5		

3.1%, with similar agreement for the inner layers. Disagreement with previous experiments [2] seems to be due to a large extent to a very strong temperature effect [3]. However, preliminary calculation of the surface thermal expansion gives only a relatively small effect, as will be shown in the next section.

Surface-phonon dispersions of Be (0001) were calculated by sampling the surface-BZ of our 12-layer slab on a 6×6 grid of points and Fourier interpolating dynamical matrices in between to obtain real-space interatomic force constants (IFC). Although the surface IFC's are well converged and recover the bulk values in the middle layers of our slab a thicker sample is necessary to decouple those surface vibrations that penetrate deeply in the bulk. The dynamical matrices of a 30-layer slab were built matching the surface IFC's to the bulk ones in the central region.

The resulting phonon dispersions are reported in Fig. 3.2 and compared with experimental data for the intense (full dots) and weak (open dots) peaks observed in Ref. [6].

Although we predict three surface modes below the bulk continuum and only one is clearly revealed in the experiment, a very good agreement is found between the experimental RW and the most surface-like calculated vibrations as can be seen in Fig. 3.3 where modes that are confined more than 30% in the first layer and are polarized perpendicularly to the surface are shown as full dots.

Note that results from truncated bulk calculations differ from experimental ones even qualitatively, giving wrong sign, and amount, for the RW dispersion from $\overline{K}$ to $\overline{M}$. As already suggested in Ref. [6], this feature is to be related to modifications of the bonding properties, due to the relaxation of the three topmost layers at the surface. However the situation is more complicated than the one described by Hannon and coworkers: we find interatomic forces near the surface continue to have a strong non-central component, comparable to the one found in the bulk.

We find that many layers are involved in the surface dynamics. To point out the surface character of the calculated modes, in Fig. 3.3 we show as open dots modes confined more than 50% in the three topmost layers. Our calculation predict two additional modes below the bulk-band edge that are not observed in Ref. [6]. These modes are peaked in sub-surface layers and have both in-plane and out-of-plane components. We suggest that they are not observed in the experiment [6] because of the strong intensity of the rather close RW, which, in the region where three modes are predicted, is for more than 70 % localized in the first layer and z-polarized. Only at the $\overline{M}$ point a shear orizontal mode has been observed [5] in the appropriate geometry. The experimental value of 50.5 meV agrees well with our result (50.0 meV). Many of the additional surface vibrations in Fig. 3.3 agree qualitatively with

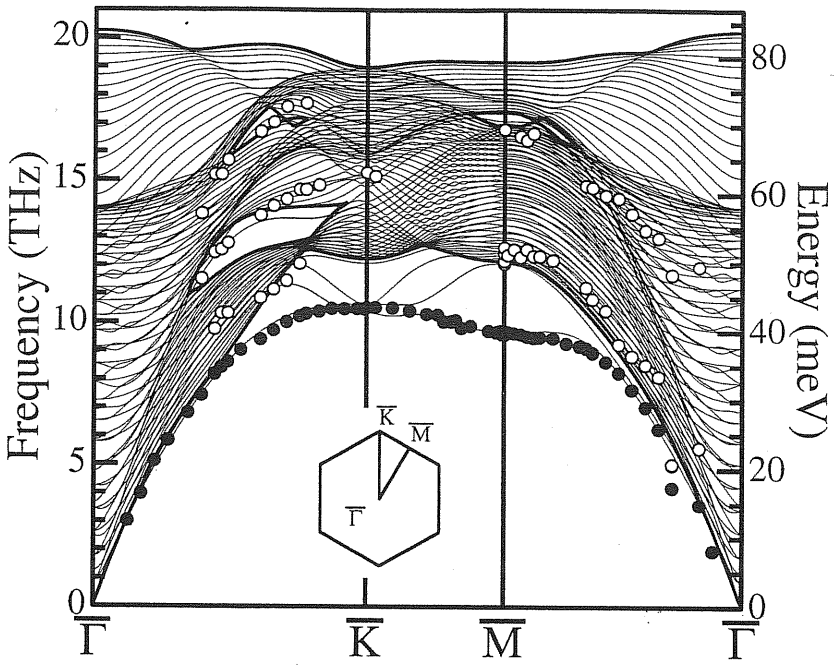

Figure 3.2: Phonon dispersion of a 30-layer slab modeling Be (0001) surface. Full and open dots are EELS data from Ref. [6] (intense and weak features, respectively). Thick lines delimit the bulk-band continuum.

weak features present in the experiment (open dots).

Finally, for long wavelenghts ($\mathbf{q} \to 0$) RW follows closely the bulk-band edge, without entering it (as was suggested instead by the model calculation in Ref. [6]) and only a minor stiffening of the RW is observed in the $\overline{\Gamma} - \overline{K}$ direction with respect to our truncated bulk calculation, as opposed to the 35% stiffening reported in [6].

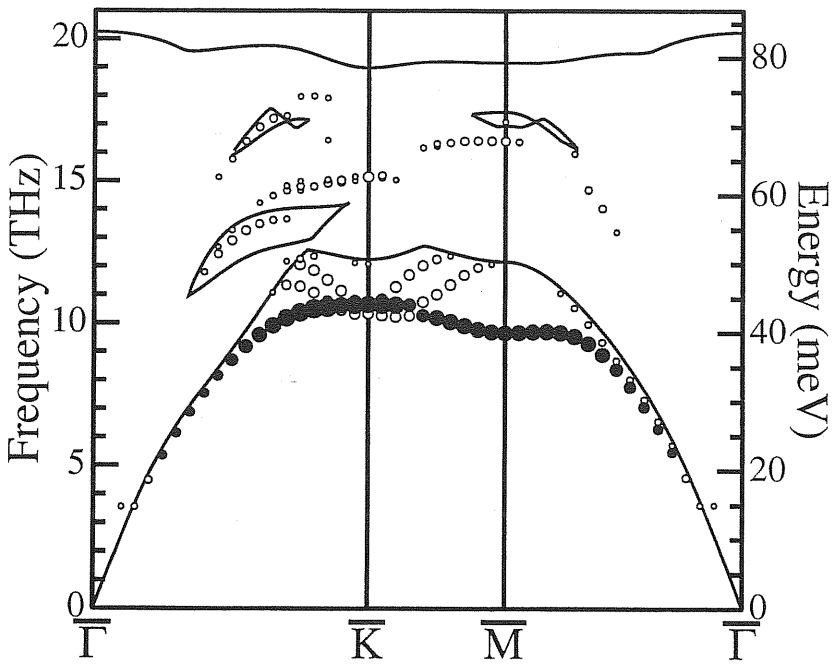

Figure 3.3: Surface character of the calculated Be (0001) vibrations: modes localized more than 50% in the three topmost layers are shown; dot size is proportional to this percentage. Full dots correspond to modes localized more than 30% in the topmost layer, polarized perpendicularly to the surface. Thick lines delimit the bulk-band continuum.

3.2 Thermal expansion

In this section the thermal expansion of Be (0001) surface is studied from first principles minimizing the free energy of the surface as a function of the interlayer separation in the quasiharmonic approximation (QHA). The QHA is applied avoiding additional simplifications [3, 19, 20] thanks to the efficient calculation by density-functional perturbation theory [11] of the needed vibrational frequencies. The ability of QHA to deal with thermal effects in bulk solids has been demonstrated in recent studies [42, 43]. The approximations involved in the determination of the surface thermal expansion within the QHA are carefully studied and an accurate sampling of the vibrational modes in the surface BZ turns out to be important in Be (0001) surface, showing that simplified calculations [3, 19, 20] may lead to inaccurate results. The full calculation does not show the large thermal expansion observed experimentally [3] and indicates that present understanding of Be (0001) surface structure is yet not fully satisfactory.

In purely harmonic crystals, ion mean positions do not change upon increasing temperature, thus crystal thermal expansion is a consequence of anharmonic terms in the interatomic potential. MD simulations account exactly for interatomic potential anharmonicity, but treats ionic degrees of freedom classically, and can give reliable results only near or above Debye temperature. The QHA provides a complementary approach, valid below the melting temperature[42, 43], for determining the temperature dependence of structural properties. In this approximation, the Helmholtz free energy, F, of a system is given by

$$F(T,\mathbf{a}) = E(\mathbf{a}) + k_B T \sum_{\nu,\mathbf{q}} \ln\left[2\sinh\left(\frac{\hbar\omega_{\nu\mathbf{q}}(\mathbf{a})}{2k_B T}\right)\right], \tag{3.1}$$

where $E(\mathbf{a})$ is the static energy of the crystal and $\omega_{\nu\mathbf{q}}(\mathbf{a})$ are the vibrational frequencies of

the system as a function of the structural parameters, $\mathbf{a}$, whose temperature dependence can be extracted from the minimization of F at any fixed temperature, T.

3.2.1 Be bulk

As a preliminary step in our study we have computed the thermal expansion of bulk Be in the *hcp* structure. We previuosly calculated the structural properties of bulk Be minimizing the static energy, $E(\mathbf{a})$ in eq. (3.1). Here, the free energy of eq. (3.1) has been considered function of the two axis lengths, a and c, and calculated on a grid of points in the two-parameter space. The vibrational contribution to the free energy resulted to be remarkably linear in the two parameters. Due to low atomic number of Be, the account of zero-point vibrations is expected to be more important than in other systems and in fact it results in a $\approx 0.7\%$ increase in both lattice parameters, further improving the agreement with experimental data: the static and the QHA calculation at T=0 give $a = 4.25$ a.u., $c/a = 1.572$ and $a = 4.28$ a.u., $c/a = 1.571$, respectively, to be compared with the experimental values, $a = 4.33$ a.u. and $c/a = 1.568$. The calculated bulk phonon dispersions for the corrected lattice parameters are similar to those obtained at the static minimum, again in good agreement with experimental data [41]. The calculated temperature variations of the bulk lattice parameters, reported in Fig. 3.4, show that QHA accounts very well for Be bulk anisothropical thermal expansion in the whole temperature range of interest.

3.2.2 Be (0001) surface

In the previous section we have shown that we have found outward relaxations, relative to the bulk, for the three topmost interlayer separations: $\Delta d_{12}/d_0 = +3.2\%$, $\Delta d_{23}/d_0 =$

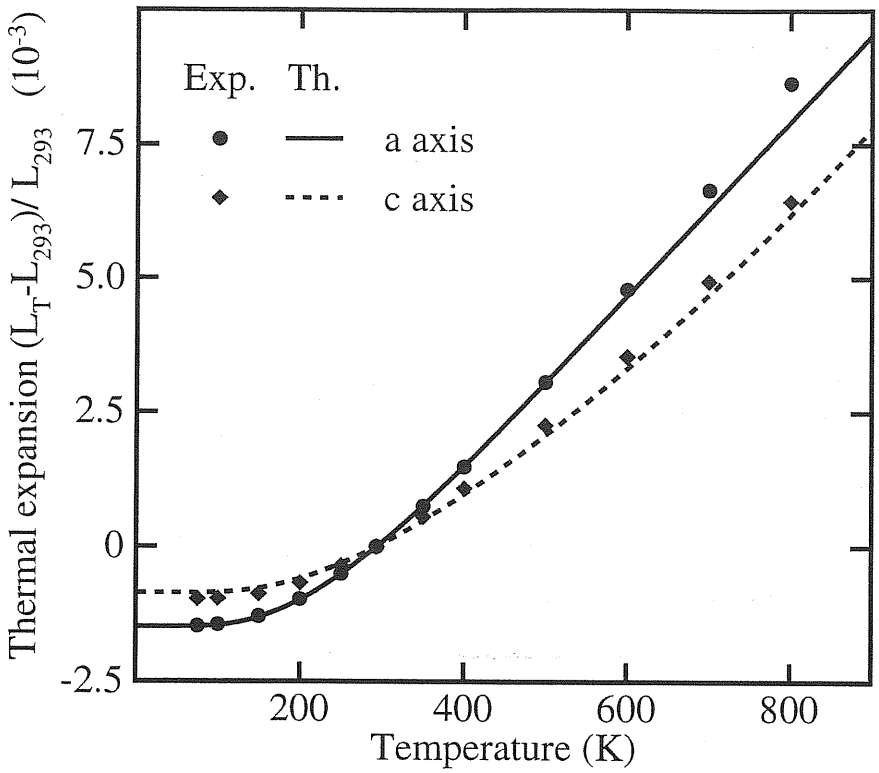

Figure 3.4: Calculated thermal expansion of bulk Beryllium. Experimental data from Ref. [44].

+1.0%, $\Delta d_{34}/d_0 = +0.4\%$. These values are found relaxing the slab from the truncated bulk positions, keeping the in-plane lattice parameter fixed at the (static) bulk value; they are in agreement with previous theoretical results [8, 10, 3] and with experimental evidence at low temperature [3].

The thermal expansion of the first surface-layer has been calculated by minimizing the QHA free energy as a function of the first interlayer separation, d_{12}. In-plane lattice parameter, $a_{||}$, and all other interatomic distances were assumed to vary according to the calculated bulk thermal expansion. In order to evaluate the free energy variation with respect to d_{12}

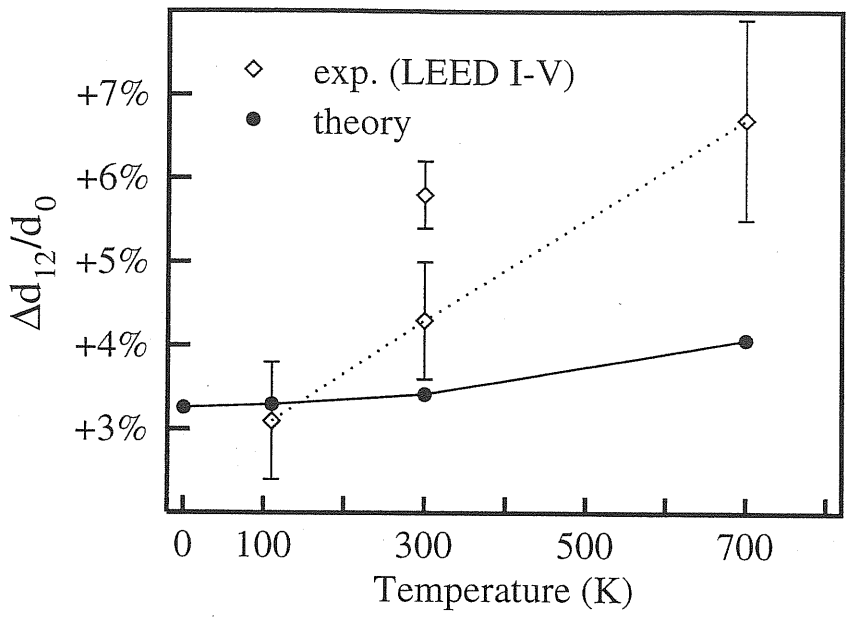

Figure 3.5: Comparison between experimental and theoretical surface toplayer expansion. The upper experimental point at room temperature is from Ref. [2], all other from Ref. [3].

and $a_{||}$, full phonon dispersions have been calculated [45] for two different values of d_{12}, corresponding to *i)* static lattice equilibrium and *ii)* the topmost layer further expanded by 2%, and two in-plane lattice parameters, corresponding to *i)* static equilibrium geometry and *ii)* the theoretical bulk value at T =700 K (a = 4.31 a.u.). The resulting vibrational free energies were interpolated (bilinearly) in between. We have examined the effect of varying the second interlayer spacing on our results and found that they are unaffected by its precise value: varying $\Delta d_{23}/d_0$ between 0 and 1.5% the total energy of the slab as a function of d_{12} does not change neither minimum position nor its curvature.

Our results are reported in Fig. 3.5 along with experimental data [2, 3]. Zero-point motion does not change significantly the first interlayer distance at zero temperature (3.3%)

with respect to the static result (3.2%). By increasing the temperature the topmost layer relaxes outward reaching 4.1% expansion, relative to the corresponding bulk value, at 700 K. At all temperatures, the expansion is mainly due to anharmonicity in the out-of-plane vibrations that accounts for about 90 % of the effect. Good agreement with experimental data is found at the lowest temperature as well as "reasonable" disagreement at room temperature, in view of the scatter between experimental data, mainly due to different experimental analysis [3]. At the highest temperature, however, the discrepancy is well beyond the experimental errorbar.

Since in Ref. [3] very good agreement has been obtained with experimental data using the simplified QHA approach introduced recently in Ref. [19, 20], we examined the effects of the approximations involved in such approach on our calculations. In Ref. [3, 19, 20] the sum over vibrational modes in the vibrational part of the free energy is replaced by the sum over three "representative wave packets" corresponding to modes at the surface BZ center where the top layer moves on a rigid substrate. Moreover the in-plane lattice parameter is kept fixed at all temperatures. In Fig. 3.6 we report the results of calculation at various degrees of approximation (full dots) together with the theoretical results from Ref. [3] for comparison (open circles). The lowest curve (full line) is our most accurate result, already shown in Fig. 3.5. Keeping fixed the in-plane lattice parameter at the static equilibrium value, still performing the full summation over vibrational modes in the free energy calculation, results in an almost rigid outward shift of the top layer (dashed line). This is a trivial effect associated with the zero-point motion tendency to make the system to expand. No large thermal effect is observed. It is only when the accurate sampling of

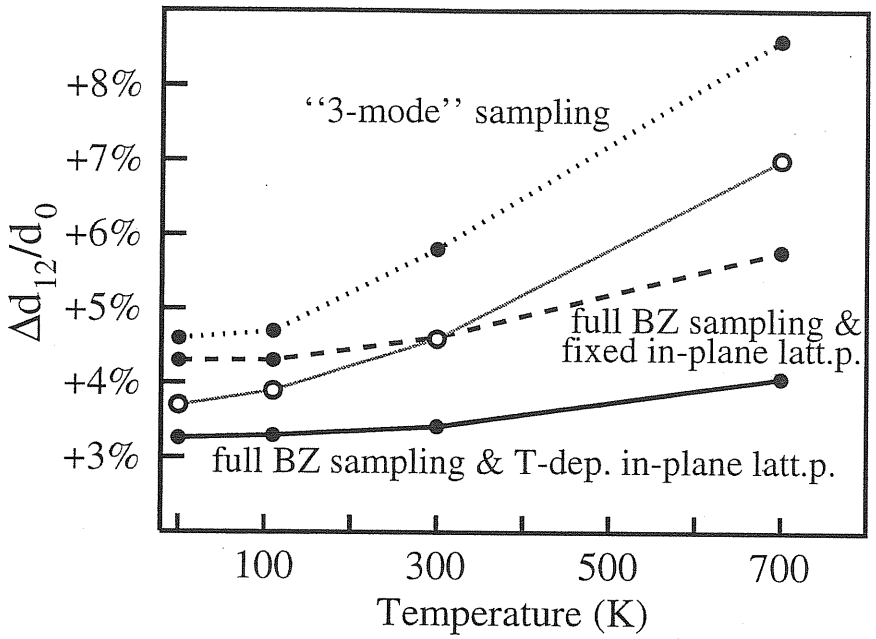

Figure 3.6: First layer thermal expansion calculated at various levels of approximation (full dots and lines, see text) compared with theoretical results from Ref. [3] (open circles).

the vibrational mode is drasticaly reduced to include only the three "representative wave packets" that a large (spurious) thermal effect appears in the calculated interlayer separation (dotted line), very similar to the results obtained with the same approximation in Ref. [3] (open circles). A similar, although less dramatic, overestimation of the surface thermal expansion due to the three-modes approximation [19, 20] is also found for Ag (111) surface [46]. In conclusion, in the case of Be (0001) surface, the better the calculation the worse is the agreement with the experiment.

This failure might suggest that QHA itself is inadequate at high temperature, due to the enhanced anharmonicity at the surface [47] with respect to the bulk case, where QHA works well. Comparison of experimental and theoretical root mean square (rms) vibrational

displacements also shows (Fig. 3.7) good agreement for the bulk values, over the whole temperature range of interest, while for the two topmost surface layers experimental rms diplacements appear to be much larger than theoretical ones. Note, however, that enhanced anharmonicity cannot be the (only) reason for these discrepancies. In fact, experimental surface-layer rms values are larger than theoretical ones even at low temperatures where QHA is expected to be accurate and accounts well for the observed surface relaxation. Note also that the *temperature dependence* of the rms displacements is well described by the calculation and the agreement with experiment could be greatly improved by a rigid shift in the theoretical, or experimental, data. It is well known (see for instance Refs. [48, 49]) that it is very difficult to tell apart static and dynamical displacements in LEED analysis and we believe that Fig. 3.7 carries strong indications that in the actual surface some degree of structural disorder is present, which has erroneously been attributed to dynamical effects. Deviations from *clean* and *flat* morphology would certainly affect the apparent rms displacements, the layer relaxations and their temperature dependence in LEED analysis of "nominally ideal" surfaces. We found, for instance, that a complete *fcc* Be adlayer, whose stacking fault cost is only 50 meV/atom in LDA, relaxes outward 2% more than the *hcp* terminated surface. Since adatoms are more stable, by $\approx$ 40 meV, in *fcc* sites than in *hcp* ones [8], mixed *fcc/hcp* layers could exist, expecially if some residual H, affecting the local energetics of defects [8] were present. More experimental and theoretical work is still needed on this issue.

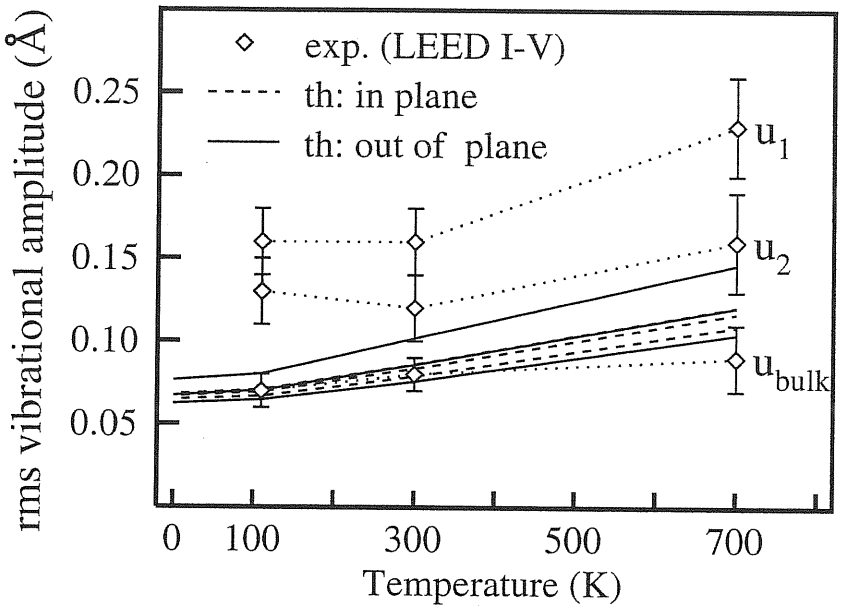

Figure 3.7: Comparison between experimental [3] and theoretical rms vibrational displacements. Outer layers display larger rms amplitudes.

Conclusions

We have shown first-principles calculation of the dynamical properties of Be (0001) surface, as obtained by state-of-the-art density-functional perturbation theory. We have calculated dynamical properties of fully relaxed 12-layer Be slabs and found significantly different results from those obtained using bulk-truncated geometry. Our results are in excellent agreement with recent EELS experiments and show that three layers are involved in the surface dynamics.

We have also shown a first-principles study, within the quasiharmonic approximation, of the thermal expansion of Be (0001) surface. The free energy is obtained from full vibrational dispersions computed by density-functional perturbation theory. Our calculation describes very well the thermal exnpasion in the bulk but we do not find the large thermal expansion recently observed experimentally and we argue that the morphology of the actual surface could be less ideal than assumed.

Bibliography

[1] G. Benedek and J.P. Toennies, Surf. Sci. **299/300**, 588 (1994); J.P. Toennies Superlatt. and Microstr. **7**, 193 (1990); K. Kress, F.W. de Wette, *Surface Phonons*, Springer Verlag (Berlin, 1991).

[2] H.L. Davis, J.B. Hannon, K.B. Ray, and E.W. Plummer, Phys. Rev. Lett. **68**, 2632 (1992).

[3] K. Pohl, J.-H. Cho, K. Terakura, M. Scheffler, and E.W. Plummer, to be published on PRL.

[4] R.A. Bartynski, E. Jensen, T. Gustafsson, and E.W. Plummer, Phys. Rev. B **32**, 1921 (1985); E.V. Chulkov, V.M. Silkin and E.N. Shirykalov, Surf. Sci. **188**, 287-300 (1987).

[5] J.B. Hannon, and E.W. Plummer, J. elct. Spect. and Related Phen. **64/65**, 683 (1993).

[6] J.B. Hannon, E.J. Mele and E.W. Plummer, Phys. Rev. B **53**, 2090 (1996).

[7] L.J. Johansson, H.I.P. Johansson, J.N. Andersen, E. Lundgren, and R. Nyholm, Phys. Rev. Lett. **71**, 2453 (1993).

[8] R. Stumpf, and P.J. Feibelman, Phys. Rev. B **51** 13748 (1995).

[9] P.J. Feibelman, Phys. Rev. B **46**, 2532 (1992).

[10] N.A.W. Holtzwarth and Y. Zeng, Phys. Rev. B **51**, 13653 (1995).

[11] S. Baroni, P. Giannozzi, and A. Testa, Phys. Rev. Lett. **58**, 1861 (1987).

[12] P. Giannozzi, S. de Gironcoli, P. Pavone and S. Baroni, Phys. Rev. B **43**,7231 (1991).

[13] M. Buongiorno Nardelli, S. Baroni, and P. Giannozzi, Phys. Rev. Lett. **69**, 1069 (1992).

[14] S. Baroni, S. de Gironcoli, and P. Giannozzi, Phys. Rev. Lett. **65**, 84 (1990); S. de Gironcoli and S. Baroni, Phys. Rev. Lett. **69**, 1959 (1992).

[15] S. Baroni, P. Giannozzi, and E. Molinari, Phys. Rev. B **41**, 3870 (1990).

[16] S. de Gironcoli, Phys. Rev. B **51**, 6773 (1995).

[17] J. Fritsch, P. Pavone, and U. Scroeder, Phys. Rev. Lett. **71**,4149 (1993); C. Bungaro, S. de Gironcoli and S. Baroni, Phys. Rev. Lett. **77**, 2491 (1996).

[18] A.P. Roy, B.A. Dasannacharya, C.L. Thaper, and P.K. Iyengar, Phys. Rev. Lett. **30**, 906 (1973).

[19] S. Narasimhan and M. Scheffler, Z. Phys. Chem. **202**, 253 (1997).

[20] J.-H. Cho and M. Scheffler, Phys. Rev. Lett. **78**, 1299 (1997).

[21] A. Kara *et.al.*, Phys. Rev. B **55**, R13440 (1997).

[22] P. Hohenberg and W. Kohn, Phys. Rev. **136**, B864 (1964).

[23] W. Kohn and L.J. Sham, Phys. Rev. **140**, A1133 (1965).

[24] J.P. Perdew and Y. Wang, Phys. Rev. B **33**, 8800 (1986).

[25] A.D. Becke, Phys. Rev. A **38**, 3098 (1988).

[26] C. Lee, W. Yang and R.G. Parr, Phys. Rev. B **37**, 785 (1988).

[27] J.P. Perdew and Y. Wang (unpublished).

[28] G.B. Bachelet, D.R. Hamann and M. Schlüter, Phys. Rev. B **26**, 4199 (1982).

[29] L. Kleinman and D.M. Bylander, Phys. Rev. Lett. **48**, 1425 (1982).

[30] S.G. Louie, S. Froyen, and M.L. Cohen, Phys. Rev. B **26**, 1738 (1982).

[31] H. Böttger, *Principles of the Theory of Lattice Dynamics* (Berlin, Akademie Verlag, 1983).

[32] X. Gonze, and J.P. Vigneron, Phys. Rev. B **39**, 13120 (1989).

[33] R.P. Feynman, Phys. Rev. **56**, 340 (1939).

[34] C.L. Fu, and K.M. Ho, Phys. Rev. B **28**, 5480 (1983).

[35] M. Methfessel, and A.T. Paxton, Rev. B **40**, 3616 (1989).

[36] C. Bungaro, S. de Gironcoli and S. Baroni, Phys. Rev. Lett. **77**, 2491 (1996).

[37] D.M. Ceperley and B.J. Alder, Phys. Rev. Lett. **45**, 566 (1980) as parametrized by J.P. Perdew and A. Zunger, Phys. Rev. B **23**, 5048 (1981).

[38] A. Dal Corso, S. Baroni, R. Resta and S. de Gironcoli, Phys. Rev. B **47**, 3588 (1993).

[39] The fitted configurations were: $2s^2$ (1.5), $2s^1 2p^1$ (0.5), $2s^1 2p^{0.5}$ (0.2), $2s^1 2p^{0.5} 3d^{0.5}$ (0.07), $2s^1 3d^1$ (0.07). The number in parentheses are the weights of each configuration used, as explained in Ref. [38].

[40] H.J. Monkhorst and J.D. Pack, Phys. Rev. B **13**, 5188 (1976).

[41] R. Stedman, Z. Amilius, R. Pauli, and O. Sundin, J. Phys. F **6**, 157 (1976).

[42] A.A. Quong and A.Y. Liu, Phys. Rev. B **56**, 7767 (1997).

[43] P. Pavone, S. Baroni, and S. de Gironcoli, Phys. Rev. B **57**, 10421 (1998).

[44] *American Institut of Physics Handbook*, edited by D.E. Gray, 3rd ed. (McGraw-Hill, new York, 1972), p. 4-120.

[45] The vibrational free energy is calculated summing over a 75×75 regular grid in the surface BZ and over all the vibrational branches of the slab obtained Fourier interpolating dynamical matrices calculated on a 6×6 grid.

[46] Xie, S. de Gironcoli, S. Baroni, and M. Scheffler to be published.

[47] R.E. Allen and F.W. de Wette, Phys. Rev. **179**, 873 (1969).

[48] B.S. Itchkawitz *et al.*, Plummer, Phys. Rev. Lett. **68**, 2488 (1992).

[49] A.F. Wright and D.C. Chrzan, Phys. Rev. Lett. **70**, 1964 (1993).